First-principles theory of the energetics of He defects in bcc transition metals

Tatiana Seletskaia,[1] Yuri Osetsky,[2] R. E. Stoller,[1] and G. M. Stocks[1]
[1]*Metals and Ceramics Division, Oak Ridge National Laboratory, Oak Ridge, Tennessee 37831-6138, USA*
[2]*Computer Science and Mathematics Division, Oak Ridge National Laboratory, Oak Ridge, Tennessee 37831-6138, USA*
(Received 14 May 2008; revised manuscript received 3 July 2008; published 6 October 2008)

Helium defect properties in V, Nb, Ta, Mo, and W were studied using first-principles electronic structure calculations. The most stable position for the He in all bcc metals is a substitutional site; the tetrahedral interstitial position is more favorable than the octahedral position. The formation energy of He substitutional defect is nearly the same for all the metals, while the formation energy of He interstitial defect strongly depends on the electronic structure of the host and insignificantly on its atomic size. The obtained He formation energies were used to calculate He binding energy to the vacancy. For V, Nb, and Ta He-vacancy binding energy is about one-half of the vacancy formation energy; for Mo and W it is about 40% higher than the vacancy formation energy. Both pair potentials and effective-medium theory fall to reproduce the preference order or the relationship between the formation energies. Calculated He formation energies and He-vacancy binding energies improve understanding of He behavior and diffusion mechanisms in metals.

DOI: 10.1103/PhysRevB.78.134103 PACS number(s): 71.55.−i, 61.82.−d

I. INTRODUCTION

Helium can have a significant impact on the mechanical properties and dimensional stability of materials used in nuclear energy systems.[1–5] Helium gas is produced in neutron-irradiated materials as a result of (n,α) transmutation reactions. Then, He atoms are deeply trapped by the vacancies, decreasing vacancy mobility and enhancing accumulation of additional vacancies and helium.[6,7] He-vacancy clustering ultimately leads to He bubble formation and can promote additional microstructural evolution by reducing vacancy-interstitial recombination. Understanding the fundamental behavior of helium in metals is a critical issue in the research and development of nuclear materials. Electronic structure calculations represent a powerful tool for obtaining information about the atomistic behavior of helium in metals such as defect formation energies and binding energies to the vacancies.

Helium is traditionally called a noble gas, implying that it is not chemically reactive with other elements. For a long time the He-metal interaction has been considered exclusively from this standpoint. The first systematic studies of He interaction with the metals were done by Wilson[8] in the late 1960s. He calculated He defect properties in metals using empirical He-metal potentials obtained by Wedepohl[9] method based on a Thomas-Fermi-Dirac formalism. The exchange energy was treated within the homogeneous gas approximation, ignoring electron correlations. The potentials were defined as a pairwise interaction energy for He-metal dimers completely ignoring bulk properties of the matrix. These empirical potentials are widely used in radiation damage simulations.[10–13]

The next step toward understanding the behavior of He in metals was associated with the development of effective-medium theory (EFMT).[14,15] EFMT is based on the assumption that the He-metal interaction is proportional to undisturbed electronic density of the atoms constituting the metal. Thus, the theory implicitly assumes He-metal pairwise interaction and ignores any distortion that the He defect can produce on the electronic structure of the host.

Subsequent elastic scattering of helium from metallic surfaces has raised questions about the correctness of the empirical approaches. Rieder *et al.*[16] studied He scattering from Rh (110) and Ni (110) surfaces and observed that He diffraction peaks are shifted away from the actual atomic positions to the bridge sites in between the atoms. The first-principles calculations of Peterson *et al.*[17] based on the density-function theory (DFT) explained this effect called as anticorrugating in terms of hybridization between He 1*s* and 3*d* orbitals of the metals. The strength of the hybridization is controlled by the geometry of *d* orbitals. Since He is a closed-shell atom and any hybridization is energetically unfavorable for it, the repulsive part of He-metal interaction potential is stronger when He is at the bridge sites rather than on top of the atoms. The authors also proposed that helium can be used for probing the substrate surface wave functions at the Fermi level.

The DFT calculations[17,18] explained the nature of anticorrugating effect and changed our view regarding helium from being chemically inactive atom to an atom that is very sensitive to its environment. Though recent DFT calculations[19] show that local-density approximation (LDA) and generalized gradient approximation (GGA) describe rare-gas adsorption site preference rather inconsistently, we are confident in using DFT-GGA for calculating He defect properties in transition metals. Since the interatomic distances in metals are small, van der Waals forces should play little role in He-metal interactions.

In this paper we present DFT-GGA calculations of He defect properties in bcc transition metals, namely, V, Nb, Ta, Mo, and W. The simplest He defects involve substitutional and interstitial positions. In the bcc structure all substitutional positions are equivalent; however, there are two (possibly) stable interstitial positions: the octahedral and the tetrahedral. These are illustrated in Figs. 1(a) and 1(b), respectively. The substitutional site, which has eight near neighbors at $0.866a_0$, has the largest free volume (a_0 is the bcc lattice spacing). The octahedral interstitial has six nearest neighbors; two of them are located at $0.5a_0$ and four of them at $0.707a_0$. The tetrahedral interstitial has four nearest neighbors at $0.559a_0$. Thus, the free volume of the octahedral de-

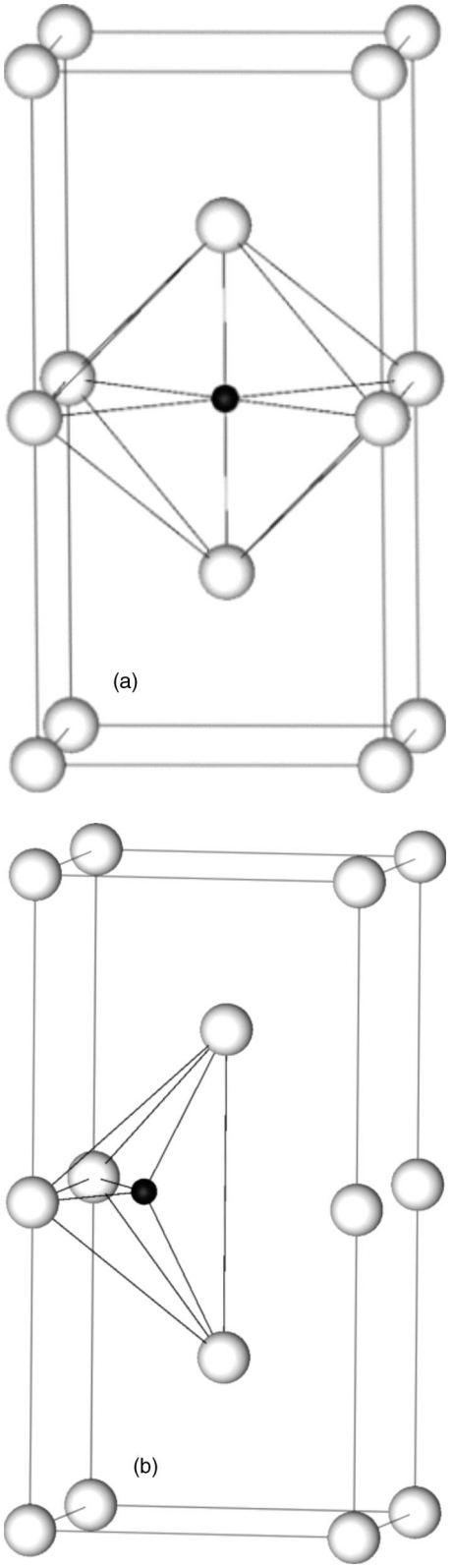

FIG. 1. The (a) octahedral and (b) tetrahedral interstitial positions in bcc structure. The black spheres show the positions of the interstitial; the white spheres are the bcc lattice sites.

fect is larger than that of the tetrahedral defect.

Previous calculations based on the pair-potential approximation and EFMT showed that He occupies the sites in order of largest free volume, namely, substitutional (sub), octahedral (octa), and tetrahedral (tetra). Furthermore, the formation energies for He defects in all bcc metals were found to be approximately the same since the models ignored the details of the electronic structure of the metals. In our previous work,[20] we considered He defect properties in iron and found that He defect behavior is governed by hybridization between He 1*s* and Fe 3*d* states near the Fermi energy level. If He is in an octahedral position, the hybridization is sufficient to cause a decrease in the magnetic moment of the neighboring Fe atoms. As a result the He octahedral position is energetically less stable than the tetrahedral one in contrast with previous work. Furthermore, the difference between the substitutional and interstitial He defect formation energies was found to be a factor of 4–9 times smaller than was predicted by empirical models. Similar results were obtained by Fu and Willaime using the SIESTA code.[21] This paper is a continuation of our research. We present systematic studies of helium interaction with the rest of the bcc transition metals excluding Cr due to disagreement between DFT with the experiments in describing its magnetic ground state.

II. METHODOLOGY

Our electronic structure calculations were performed using the Vienna *ab initio* simulation package (VASP).[22–24] Solution of the Kohn-Sham equations[25] was carried out self-consistently using a plane-wave basis set with projector augmented wave (PAW) pseudopotentials.[26,27] Exchange and correlation functionals were taken in a form proposed by Perdew and Wang (PW91) (Ref. 28) within the GGA.

The calculations were performed using supercell models of the defect structures in which He atoms are placed at the appropriate positions of a large cell that is an $n \cdot n \cdot n$ repeat of the underlying bcc structure with the equilibrium lattice parameter. Then, the atomic coordinates and volume were relaxed to minimize the forces and pressure. The energy of an isolated He atom is obtained by considering a cubic unit cell with a significantly large lattice parameter, namely, 10 Å, and one *k*-point in the irreducible Brillouin zone.

The following definitions are used throughout the paper. The relaxation energy of a crystal is determined as a difference between the total energy of a crystal before and after relaxation. The relaxation volume is determined similarly. In order to be comparable, the formation energies of He interstitial and substitutional defects are defined for the same initial atomic configuration that is a perfect bcc crystal with an isolated He atom. The formation energy of He interstitial is

$$E^f_{\text{interstitial}} = E_{Nm,\text{He}} - NE_m - E_{\text{He}}, \tag{1}$$

where N is the number of metal atoms in the initial and final supercells, E_m is the energy per atom of the perfect bcc lattice, and E_{He} is the energy of an isolated He atom. Creating a He substitutional defect causes also a creation of a vacancy. The formation energy in this case is

$$E^f_{\text{sub}} = E_{(N-1)m,\text{He}} - (N-1)E_m - E_{\text{He}} - E^f_{\text{vac}}, \tag{2}$$

where E^f_{vac} is the formation energy of a vacancy. The binding energy of a He atom to a vacancy is defined straightforward

TABLE I. Calculated and experimental equilibrium atomic volumes, Ω_0 (Å^3), bulk moduli, B_0 (GPa), vacancy formation energies, E^f_{vac} (eV), and vacancy formation volumes, Ω^f_{vac} (Ω_0), for bcc *d*-transition metals.

	PAW-GGA				FP-LMTO-GGA[a]			Expt.[b]		
	Ω_0	B_0	E^f_{vac}	Ω^f_{vac}	Ω_0	B_0	E^f_{vac}	Ω_0	B_0	E^f_{vac}
V	13.2	153	2.28	0.70	13.3	134	2.55	13.9	157	2.1–2.2
Nb	18.2	179	2.62	0.60	18.2	157	2.88	18.0	173	2.6–3.0
Ta	18.1	203	2.86	0.70	18.1	183	3.20	17.9	194	2.8–3.1
Mo	15.7	268	2.62	0.51	15.7	266	2.90	15.5	265	2.6–3.2
W	15.8	334	3.12	0.70	16.2	310	3.60	15.9	314	3.5–4.1

[a]Reference 30.
[b]References 31 and 32.

as the energy difference between interstitial and substitutional positions,

$$E_{\mathrm{bind}} = E^f_{\mathrm{interstitial}} - E^f_{\mathrm{sub}}. \tag{3}$$

The energy of interstitial migration is somewhat less than the energy difference between the octahedral and tetrahedral positions.[21] Then, the He dissociation energy is defined as the binding energy plus the energy of interstitial migration.

Since the defect formation energies given by Eqs. (1) and (2) represent a small difference between large numbers, one has to be careful about calculational settings. To examine the impact of simulation cell size, we carried out calculations using both 54 and 128 atom supercells. Larger supercells were not considered due to the substantial increase in the computational time. For every atomic configuration we tested the energy convergence with respect to the number of *k* points used in the integration over the Brillouin zone and the basis-set cutoff energy. Brillouin-zone sampling was performed using the Monkhorst-Pack scheme.[29] For the 54-atom supercell, we took a $6\times6\times6$ *k*-point mesh that produced 40 *k* points for interstitial defects and 20 *k* points for substitutional defect and perfect bcc lattice. These numbers were correspondingly twice smaller for 128-atom supercell calculations. The minimal cutoff energy providing energy convergence was found to be 350 eV for all the metals.

In this paper, unless otherwise specified, we present the results obtained from 128-atom supercell calculations including both atomic and volume relaxations. Changing the supercell size from 54 to 128 atoms decreases He formation energies by up to 0.2 eV; however, the relative energy differences between the defect configurations change by at most 0.1 eV. In addition we performed atomic relaxation at constant volume. In this case the calculated energies are noticeably higher than those in Table I. The extreme case is a He defect in W, where performing volume relaxation lowers the formation energies by 0.4 eV. But even in this case the ratios between the energies are weakly affected. Thus, when the volume of the supercell is fixed, the energy difference between He octahedral and tetrahedral defects decreases by 0.07 eV comparing to the calculations with the relaxed volume, and the He-vacancy binding energy decreases by 0.15 eV in this case. We conclude by noting that calculations based on changing the supercell size and carrying out the atomic relaxation at constant volume preserve the relationship between He formation energy with the high accuracy.

Before considering He defect in bcc metals, we used PAW pseudopotentials to calculate the basic physical properties of the pure metals. In Table I we present calculated equilibrium atomic volume, bulk modulus, vacancy formation energy, and vacancy formation volume. The results of full-potential GGA calculations[30] and experimental data[31,32] are given for comparison. The bulk moduli were obtained by expanding and contracting the bcc unit cell within 10% of its equilibrium lattice parameter. Then we performed Birch fitting[33] of the uniform expansion curve and found the bulk modulus at experimentally measured lattice constant. The vacancy formation energy and vacancy formation volume were calculated by the same procedure as in reference.[30]

For Nb, Ta, and Mo our calculations show a very good agreement with full-potential calculations and the experiment. Both calculations overestimate the atomic volumes by less than 1%. The bulk moduli agree with the experiment within 5%. The vacancy formation energies calculated by PAW-GGA method are lower than the values obtained in the full-potential calculations, but they are still within the uncertainty of the experiment. The calculated atomic volume of V is 5% smaller than the experimentally measured value and the vacancy formation energy is overestimated by 0.08 eV. The largest discrepancy between calculations and the experiment is found for W. In the case of W, the calculated bulk modulus is overestimated by 6% comparing with the experiment, but the vacancy formation energy is by 0.4 eV smaller than its measured value. The later introduces an error of the same order in our calculation of He substitutional formation energy in W and in He dissociation energy. However, as we will see later, the dissociation energy of He in W is a big number and PAW-GGA method allows us to determine it with the relative accuracy of 10%.

III. RESULTS

Table II shows the results of our first-principles calculations of the He formation energy in bcc transition metals for octahedral, tetrahedral, and substitutional positions. For interstitial defects, the volume change due to atomic relaxation, $\Delta\Omega$, is determined with respect to perfect bcc crystals;

TABLE II. The volume change, $\Delta\Omega$ (Ω_0), relaxation, E^f (eV), and formation energies, E^f (eV), of He defect in transition bcc metals.

		$\Delta\Omega$	E_{rel}	E^f	E^f_{pair} [a]	E^f_{EFMT} [b]
V	He_{octa}	0.27	1.93	3.17	4.61	
	He_{tetra}	0.26	1.19	2.94	4.74	
	He_{sub}	0.62	0.39	2.30	1.65	
	$\text{He}_{\text{subdrift}}$	0.62	0.56	2.03		
Nb	He_{octa}	0.31	1.51	3.26		3.04
	He_{tetra}	0.31	0.94	3.05		3.10
	He_{sub}	0.19	0.07	1.38		
Ta	He_{octa}	0.32	1.83	3.42	4.23	
	He_{tetra}	0.32	1.27	3.16	4.22	
	He_{sub}	0.17	0.17	1.75	0.93	
Mo	He_{octa}	0.28	1.75	5.33	4.91	4.46
	He_{tetra}	0.28	1.39	5.16	5.14	4.44
	He_{sub}	0.22	0.07	1.76	1.04	1.59
W	He_{octa}	0.37	1.82	6.39	5.47	4.60
	He_{tetra}	0.39	1.61	6.15	5.71	4.58
	He_{sub}	0.40	0.47	1.38	1.05	1.27

[a]Reference 8.
[b]References 14 and 15.

for substitutional defects, $\Delta\Omega$ is calculated with respect to the lattices relaxed around the vacancy. Table II contains also the formation energies calculated within pair potential[8] and EFMT (Refs. 14 and 15) models for comparison. The numerical values of He defect formation energies are in a relatively good agreement with the results of the similar work.[34] In the table the metals are placed in the following sequence. First, we put the elements that belong to the same column of the Periodic Table. Inside each group of these elements, they are placed in ascending order of the row number.

We find that the He defect induces strong atomic relaxation with the atomic shells neighboring the He impurity relaxing outward for all defects and metals considered. For He in the interstitial position, relaxation decreases the formation energies by more than 26%. For all of the metals considered, the volume expansion associated with the He interstitial defect is essentially the same for both octahedral and tetrahedral configurations. Not surprisingly, placement of He into the vacancy also causes lattice expansion. This expansion is largest in V and W, where we also find the largest relaxation energy. For all the metals, the volume change resulting from the He substitution is smaller than the vacancy formation volume (compare Ω^f_{vac} of Table I with $\Delta\Omega$ of Table II). Of course, relative to the pure solid, substitution of metal atom by He results in an overall reduction in the supercell volume consistent with the fact that the He atom is much smaller than the metal atom which it is replacing.

From Table II one can see that He substitutional defect is the most stable for all metals considered. The formation energy of this defect varies between the different metals by only 0.65 eV which is much smaller than the variation in energy (~3 eV) associated with the He interstitial defects. In all cases, the tetrahedral is the most stable He interstitial

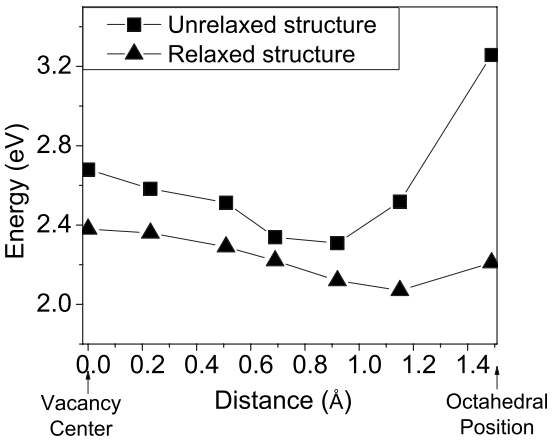

FIG. 2. Energy profile of He substitutional formation energy along [100] path from the center of the vacancy to the octahedral position.

position. This finding conflicts with the result of empirical models which predict the octahedral defect to be the most stable. The energy difference between He octahedral and tetrahedral positions varies from 0.14 eV for W to 0.26 eV for Ta. These energies agree quite well with an experimental value in the range of 0.24–0.32 eV that was obtained from atom-probe microscopy studies[35] and estimates of enthalpy change in migration. Of particular note is the more than doubling of the formation energy of He tetrahedral defect, from 3.04 to 6.15 eV, between V and W. As will be discussed later, the explanation of this large difference lies in differences in the electronic structure of the host metals.

From Table II it can be seen that both empirical models fail to reproduce the defect preference order. The pair potential model[8] gives about the same formation energies for all the hosts contrary to the roughly factor of 2 difference between V and W found in the first-principles results. The EFMT (Refs. 14 and 15) provides a better description of the He defect than the pair potential model. For He interstitial defects in Nb and He substitutional defects in Mo and W the EFMT results only slightly differ from our PAW-GGA calculations. Thus, the description of He-metal interaction in terms of the undisturbed electronic densities can be acceptable in this cases. The EFMT model in general fails once the electronic structure effects become strong. In Table II one can see that in case of Mo and W the EFMT calculations underestimate the He interstitial defect energies by more than 0.7 eV.

As is highlighted in Table II the He substitutional atom in V behaves quite differently from that in the remaining metals. Interestingly, when He atom is in a vanadium vacancy and atomic relaxation is performed the energy minimum corresponds to an atomic configuration with the He atom displaced from the vacancy center toward the octahedral position. The first-principles calculations yield a displacement (*drift*) of 1.2 (Å) which is a large fraction (37%) of V lattice parameter. In Table II the drifted He substitutional defect is denoted by $\text{He}_{\text{subdrift}}$ from which it can also be seen that the drift decreases the energy by 0.21 eV. To expand on this result, in Fig. 2 we show how the formation energy varies as the He substitutional defect is displaced from the center of

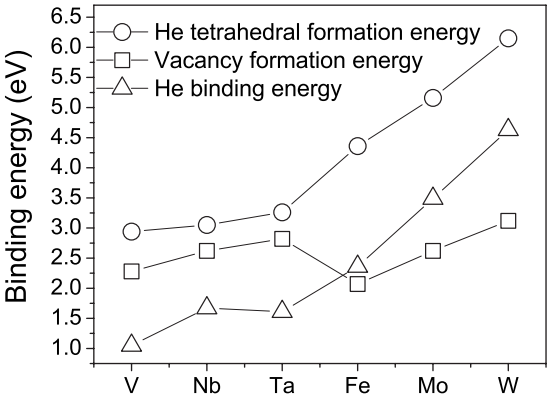

FIG. 3. Calculated formation energies of He tetrahedral defect, vacancy formation energies, and He-vacancy binding energies depending on the type of metal.

the vacancy toward the octahedral position. The two curves show calculations for a frozen lattice (squares) and calculations (triangles) in which atomic relaxation around a fixed He atom is taken into account.[36] From Fig. 2 one can see that even in unrelaxed lattice case the displaced position is energetically more favorable—by 0.12 eV. After atomic relaxation the energy minimum moves even closer to the octahedral position with a further decrease in the energy. Clearly, the He displacement is a purely quantum-mechanical effect and therefore was not observed in previous classical calculations. It should also be noted that this displacement effect is specific to He in V; in all the other metals the center of the vacancy is the most stable position for both relaxed and unrelaxed structures.

Using the He defect formation energies presented in Table II it is straightforward [Eq. (3)] to calculate the binding energy of He to a vacancy. The results are shown in Fig. 3 as triangles. Because the formation energies of He substitutional defect (shown as squares in Fig. 3) are rather similar for all of the hosts, the interelement variation in the He binding energy mainly reflects differences in He interstitial formation energies (shown as circles in Fig. 3). A point to note is that the He binding energy changes rapidly going across a column of the Periodic Table while it differs only slightly between metals that belong to the same column. The value of the binding energy of He in Fe taken from our previous work[20] lies between the energies calculated for V and Mo groups. As we will show later, the variations in defect binding energies that we have just described find a ready explanation in terms of the underlying electronic structure of the hosts.

Given that He is produced in metals during irradiation which simultaneously produces vacancies, it is interesting to look at the relationship between He binding energies and vacancy formation energies shown in Fig. 3. In V, Nb, and Ta the He-vacancy binding energy is about one-half the vacancy formation energy; in Fe the two values are about the same, and in Mo and W the He-vacancy binding energy is 40% higher than the vacancy formation energy.

A detailed comparison of our calculated He dissociation energies with the results of the previous calculations as well as experiment is presented in Table III. Since in the pair-potential model electronic structure effects were not taken into account, the He defect behavior found in these studies is similar for all bcc metals; EFMT calculations strongly overestimate the dissociation energies of Fe, Mo, and W and give unrealistically small energy for Nb. Our calculations show that He binding energy increases as you go across the periodic table from V to W. The experimentally measured He dissociation energies for Fe, Mo, and W exhibit similar behavior. For V and Fe desorption measurements[7] give similar values of He dissociation energies, while our calculations indicate that there is an energy difference about 1 eV. Unfortunately, the desorption experiments are unable to capture all the details of the atomistic behavior; therefore it is difficult to say what exactly causes this disagreement. Diffusion of He in metals involves He evolution in a complex environment of defects induced during implantation and thermal vacancies formed during the high-temperature desorption measurements. This involves a number of interactions and reactions of He with the other defects which are impossible to predict without detailed simulations using an atomistic model. Here is worthwhile to note that such simulations could become possible if one were to use the internally self-consistent set of He defect calculations in bcc transition metals presented here to construct interatomic potentials for He-metal interactions and to employ them in large-scale atomistic simulations to investigate He diffusion in metals and its impact on microstructure evolution of the metals under irradiation.

TABLE III. He dissociation energy (eV) calculated using PAW-GGA pseudopotentials, pair potentials, effective-medium theory, and measured experimentally.

	PAW-GGA	Pair potential[a]	EFMT[b]	Expt.
V	1.28	3.65		1.4 ± 3 [c]
Nb	1.67		0.06	
Ta	1.61	3.93		
Fe	2.36	3.75	4.27	1.4 ± 3 [c]
Mo	3.67	3.04	5.45	3.8[d]
W	5.1	3.05	6.81	4.0[e]

[a]Reference 8.
[b]References 14 and 15.
[c]Reference 7.
[d]Reference 37.
[e]Reference 38.

IV. DISCUSSION

In the following we analyze the electronic structure of the various He defects and hosts in an attempt to shed light on three questions: (1) what underlies He site-preference order in the different transition metals; (2) what are the origins of the variations in interstitial He defect energies across the various host metals; (3) why does the He substitutional defect drift away from the vacancy center in V.

In Figs. 4(a) and 4(b) we present site-projected electronic densities of states (DOS) of He substitutional and tetrahedral

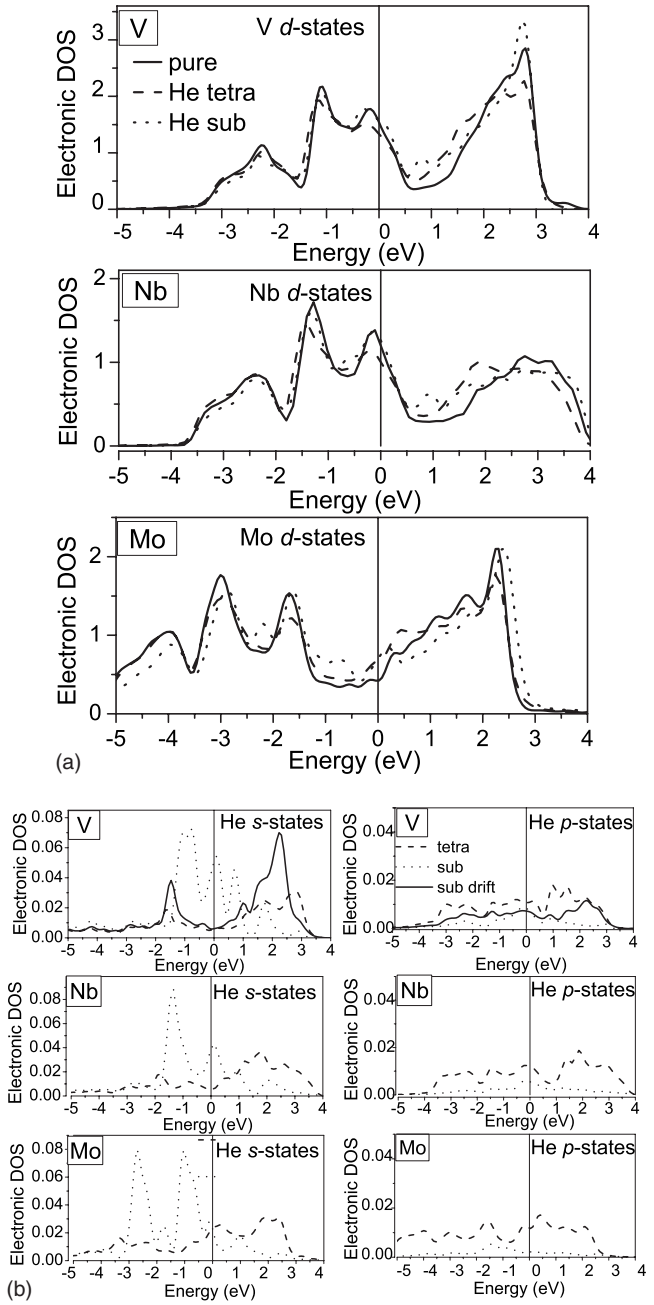

FIG. 4. (a) Local DOS for V and Mo atoms and (b) local DOS for He defect. In (a) the solid line shows the DOS of pure metals. The dashed and dotted lines represent the DOS of metal sites with the He at tetrahedral and substitutional positions, respectively. In (b) the dashed and dotted lines represent the DOS of He octahedral and substitutional defects, respectively. The solid line shows the DOS of He substitutional defect in V after its drift from the vacancy center. The Fermi energy of the supercell with the He defect is 0.00 eV.

defects in V, Nb, and Mo for the components of the DOS that change most between different defect environments. In Fig. 4(a) we show the *d*-projected DOS of the metal atom closest to the He defect and, in Fig. 4(b), the *s*- and *p*-projected DOS of the He defect itself. The He atom does not gain any *d* states. For comparison we also show, by the solid line in Fig. 4(a), the *d*-projected DOS of the pure metals. We focus on

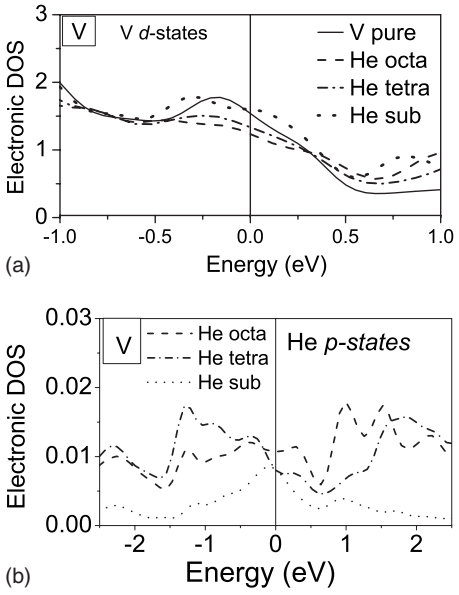

FIG. 5. (a) Local DOS for V atom and (b) local DOS for He defect. In (a) the solid line shows *d* projected DOS of pure V. The dashed line and the dashed line with the dots represent the DOS of metal sites with the He at octahedral and tetrahedral positions, respectively. The dotted line shows the DOS of V with He substitutional defect. The *p*-projected DOS of He are shown in (b). The Fermi energy of the supercell with the He defect is 0.00 eV.

the DOS of V and Nb to illustrate the similarities in their electronic structure and on Mo to highlight the differences with the previous two. As for the rest of the metals, the electronic structure of He defect in Ta resembles the one in Nb and the DOS of He defect in W is very similar to the He defect in Mo. The DOS of He octahedral defect are only slightly different from the He tetrahedral DOS. In Figs. 5(a) and 5(b) we present enlarged *d*-projected DOS of V site and *p*-projected DOS of He substitutional, tetrahedral, and octahedral defects to demonstrate the differences in He octahedral and tetrahedral defects behaviors.

In Fig. 4(a) one can see that the He defect produces distortion of the DOS of the neighboring metal atoms that indicates the ongoing hybridization. Since He is a closed-shell atom and any hybridization is energetically unfavorable for it, larger distortion of the DOS at the metal site corresponds to the larger formation energy of He defect. The electronic DOS of He atom shown in Fig. 4(b) also change due to hybridization. The He atom acquires some *s* and *p* states near the Fermi energy level. Though the absolute values of He DOS are relatively small (integrated DOS at He site are less than 0.14 electrons), they cannot be neglected. Since the relaxation around He substitutional defect is small (the relaxation energy never exceeds 30% of the formation energy and the displacement of the first neighbors is less than 6% of the lattice parameter), we conclude that the large values of the formation energies (for all the metals larger than 1.3 eV) come from the electronic hybridization. The He substitutional defect gets mostly *s* states near the Fermi energy level since the vacancy has the largest free volume and symmetric environment. The He tetrahedral defect acquires some limited *p* character. Although *s*-projected He DOS are generally

larger than the *p* DOS, having *p* states in the neighborhood of the Fermi energy is particularly unfavorable, given that He is an atom with a completed spherically symmetric *s* shell. If this is the case, then the larger the He *p* DOS at the Fermi energy level, the less energetically favorable is the corresponding He defect configuration. In Fig. 5(b) one can see that He octahedral DOSs are higher than the DOS of the tetrahedral defect and both interstitial defects have higher DOS at the Fermi energy than the DOS of He substitutional defect in agreement with the order of the preference of He in metals, namely, sub, tetra, and octa. We conclude that the hybridization between transition metals *d* states and He *p* states is responsible for site-preference order of He in metals and is the reason for large He formation energies. A similar result was previously obtained for He defect in Fe.[20]

While He site-preference order is the same in all considered transition metals, the values of the formation energies of He interstitials are different for the metals of V and Mo columns and only in V do we observe the drift of the He substitutional atom from the vacancy center. To find the reasons for these phenomena we turn to analyzing the electronic structure of the metals. As is well known, the electronic structure of the bcc transition metals is characterized by a hybridization gap between low-energy bonding states and high-energy antibonding states [see Fig. 4(a)]. For V, Nb, and Ta, the Fermi energy lies at the top of the bonding states (at the bottom of the hybridization gap), while for Mo and W, the Fermi energy lies at the bottom of the antibonding states (at the top of the hybridization gap). It is interesting to note that spin-polarized Fe represent an intermediate case between V and Mo columns. Its majority (spin up) *d* band is full and the Fermi energy lies in the middle of the hybridization gap in the minority (spin down) DOS.

Studies of the bonding charge densities show that the location of the Fermi energy strongly correlates with the directionality of atomic bonding and the density of the interstitial charge. While V, Nb, and Ta have high electron density at the Fermi energy level, Mo and W have a much lower Fermi energy charge density. In Fig. 6 we show the spatial distribution of the charge density of V in 50 meV energy below the Fermi energy. The charge is concentrated at the atomic sites and it is also spread between the atoms along the atomic bonds. One can see that there is almost no Fermi energy charge density around the octahedral position denoted in the Fig. 6 by label X. In Mo and W the situation is different. In these metals the corresponding *d* states are located well below the Fermi energy, the result being that the charge distribution is more uniform in the interstitial region and consequently has a larger value.

The hybridization between metal and He electronic states can also be visualized in charge-density plots. In Figs. 7(a) and 7(b) we show the charge density corresponding to the He octahedral defect in the relaxed structures in V and Mo, respectively. In these figures one can see that He defect polarizes its first and second neighbors and is itself polarized. The metal atoms loose the charge from the e_g atomic orbitals and gain it in the atomic orbitals with t_2g symmetry. Clearly, the atoms of Mo become more strongly polarized than those of V. In addition, the He interstitial atom is also more strongly polarized. Since the charge density in the interstitial region is higher in Mo than in V, the He atom looses more of its charge which determines the relationship between the formation energies of He interstitial defects in this metals. In V, Nb, and Ta the He polarization is small and the He formation energies are almost the same in all of these metals. On the other hand, in Mo and W the polarization is significant due to the larger interstitial charge density and the formation energies are significantly larger than the former group. Because

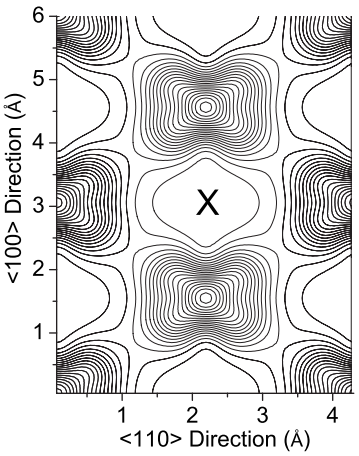

FIG. 6. The charge density of V in 50 meV energy window at the Fermi level in the [110] plane. The lines represent contours of equivalent charge density. The cross shows the location of octahedral interstitial positions.

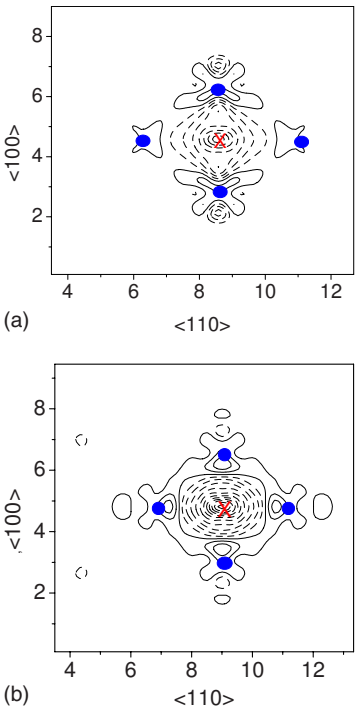

FIG. 7. (Color online) The change in the charge density of (a) V and (b) Mo after inserting He in an *octahedral* position. The lines represent contours of equivalent charge density. Solid lines indicate an increase in charge density and dashed lines represent charge depletion. The cross indicates the position of He and filled circles specify the position of neighboring metal sites.

the interstitial charge density in W is larger than in Mo, as befits the more extended 5*d* states of W relative to the 4*d* states of Mo, this results in a yet larger formation energy of He interstitial.

In the case of the He substitutional defect the situation is opposite. When the original atom is removed from the lattice, the vacancy is filled with the electronic charge from the surrounding metal atoms. Since atomic bonding in V has a more pronounced directional character, its vacancy has a higher charge density than the vacancies of the other metals. The energy of the electronic charge in the vacancy lies in the vicinity of the Fermi level; therefore, the He substitutional defect must interact with it. As one can see in Fig. 4(b), the *s* states corresponding to a He placed in V vacancy have sharp peak at the Fermi energy level; in Nb this peak becomes smaller and in Mo He *s* states are located below the Fermi energy. The larger are the DOS at the Fermi energy level, the higher is the formation energy of the corresponding defect configuration. Particularly in V, He substitutional energy is so high that it makes this configuration unstable and He drifts away from the vacancy center toward the octahedral position. The drift lowers the formation energy of the defect by 0.27 eV and eliminates the DOS peaks at the Fermi energy level. The same effect does not happen in Nb which has the same electronic structure because Nb has slightly larger atomic radius and therefore higher interstitial charge density. If a He substitutional atom is displaced from the center in Nb vacancy, it acquires more of the *p* states and the He formation energy increases.

V. SUMMARY

In summary we note that despite being a closed-shell atom the relative stabilities of the various defects are determined by the interaction between the He defect atom and the charge density of the host system. Since the charge density is higher in the interstitial region than in the vacancy, the He defect prefers to occupy a substitutional position in all the metals. The hybridization between metal *d* states and He *p* states is responsible for He tetrahedral site preference over the octahedral site. The formation energy of He substitutional defect is nearly constant for all the metals; the formation energy of He interstitial depends on the electronic structure of the host. In V, Nb, and Ta the interstitial formation energies are nearly the same and are much smaller than He formation energies in Mo and W.

Investigation of He defect properties in metals illustrates the power of first-principles methods. Both pair potentials and effective-medium theory fail to reproduce He defect preference order or the relationship between formation energies. Calculated He defect formation and He-vacancy binding energies improve our understanding of He behavior and diffusion mechanisms in metals with significant implications of understanding their irradiation response. Parametrization of *ab initio* results to develop empirical potentials will permit molecular-dynamics (MD) investigation of diffusion and bubble behaviors. Further work is planned to apply similar methods to investigate hydrogen in metals and synergistic effects of H and He. Such studies are important for understanding of He diffusion and He bubble formation in the metals under irradiation.

ACKNOWLEDGMENTS

This research was sponsored by the Division of Materials Sciences and Engineering and the Office of Fusion Energy Sciences, U.S. Department of Energy under Contract No. DE-AC05-00OR22725 with UT-Battelle, LLC.

[1] K. Farrell, P. J. Maziasz, E. H. Lee, and L. K. Mansur, Radiat. Eff. **78**, 277 (1983).
[2] R. E. Stoller, J. Nucl. Mater. **174**, 289 (1990).
[3] R. E. Stoller and G. R. Odette, J. Nucl. Mater. **154**, 286 (1988).
[4] R. E. Stoller, P. J. Maziasz, A. F. Rowcliffe, and M. P. Tanaka, J. Nucl. Mater. **155-157**, 1328 (1988).
[5] B. van de Schaaf, D. S. Gelles, S. Jitsukawa, A. Kimura,R. L. Klueh, A. Moslang, and G. R. Odette, J. Nucl. Mater. **283-287**, 52 (2000).
[6] M. B. Lewis and K. Farrell, Nucl. Instrum. Methods Phys. Res. B **16**, 163 (1986).
[7] R. Vassen, H. Trinkaus, and P. Jung, Phys. Rev. B **44**, 4206 (1991).
[8] W. D. Wilson, in Proceedings of the Conference on Fundamental Aspects of Radiation Damage in Metals, edited by F. W. Young and M. T. Robinson, p. 1025, USERDA Report No. USERDA-CONF-751006-P2, 1979.
[9] P. T. Wedepohl, Proc. Phys. Soc. **92**, 79 (1967).
[10] L. M. Caspers, M. R. Ypma, A. Van Veen, and G. J. Van der Kolk, Phys. Status Solidi A **63**, K183 (1981).
[11] K. Morishita, R. Sugano, B. D. Writh, and T. Diaz de la Rubia, Nucl. Instrum. Methods Phys. Res. B **202**, 76 (2003).
[12] R. J. Kurtz and H. L. Heinisch, J. Nucl. Mater. **329-333**, 1199 (2004).
[13] L. Ventelon, B. Wirth, and C. Domain, J. Nucl. Mater. **351**, 119 (2005).
[14] M. Manninen, J. K. Norskov, and Cyrus Umrigar, J. Phys. F: Met. Phys. **12**, L7 (1982).
[15] B. Bech Nielsen and A. van Veen, J. Phys. F: Met. Phys. **15**, 2409 (1985).
[16] K. H. Rieder, G. Parschau, and B. Burg, Phys. Rev. Lett. **71**, 1059 (1993).
[17] M. Petersen, S. Wilke, P. Ruggerone, B. Kohler, and M. Scheffler, Phys. Rev. Lett. **76**, 995 (1996).
[18] N. Jean, M. I. Trioni, G. P. Brivio, and V. Bortolani, Phys. Rev. Lett. **92**, 013201 (2004).
[19] Juarez L. F. Da Silva and C. Stampfl, Phys. Rev. B **77**, 045401 (2008).
[20] T. Seletskaia, Y. Osetsky, R. E. Stoller, and G. M. Stocks, Phys. Rev. Lett. **94**, 046403 (2005).
[21] C. C. Fu and F. Willaime, Phys. Rev. B **72**, 064117 (2005).
[22] G. Kresse and J. Hafner, Phys. Rev. B **47**, R558 (1993).

[23] G. Kresse and J. Furthmüller, Phys. Rev. B **54**, 11169 (1996).
[24] G. Kresse and J. Furthmüller, Comput. Mater. Sci. **6**, 15 (1996).
[25] W. Kohn and L. J. Sham, Phys. Rev. **140**, A1133 (1965).
[26] P. E. Blöchl, Phys. Rev. B **50**, 17953 (1994).
[27] G. Kresse and D. Joubert, Phys. Rev. B **59**, 1758 (1999).
[28] J. P. Perdew, J. A. Chevary, S. H. Vosko, K. A. Jackson, M. R. Pederson, D. J. Singh, and C. Fiolhais, Phys. Rev. B **46**, 6671 (1992); **48**, 4978(E) (1993).
[29] H. J. Monkhorst and J. D. Pack, Phys. Rev. B **13**, 5188 (1976).
[30] Per Söderlind, L. H. Yang, John A. Moriarty, and J. M. Wills, Phys. Rev. B **61**, 2579 (2000).
[31] C. Kittel, *Introduction to Solid State Physics*, 6th ed. (Wiley, New York, 1986).
[32] J. Donohue, *The Structure of the Elements* (Wiley, New York, 1974).
[33] F. Birch, J. Geophys. Res. **83**, 1257 (1978).
[34] F. Willaime and C. C. Fu, *Structural and Refractory Materials for Fusion and Fission Technologies*, MRS Symposia Proceedings No. 981 (Materials Research Society, Pittsburgh, 2007), Paper No. 0981-JJ05-04.
[35] A. Wagner and D. N. Seidman, Phys. Rev. Lett. **42**, 515 (1979).
[36] Note that these calculations were performed for 54-atom supercell and as a result the values for the equilibrium differ slightly from the data presented in Table II.
[37] A. van Veen, J. H. Evans, W. Th. M. Buters, and L. M. Caspers, Radiat. Eff. **78**, 53 (1983).
[38] E. V. Kornelsen, Radiat. Eff. **13**, 227 (1972).